Determination of Low-Strain Site-Amplification Factors in the Salt Lake Valley, Utah, Using ANSS Data

Kris L. Pankow and James C. Pechmann, University of Utah Seismograph Stations,
135 South 1460 East, Room 705 WBB, Salt Lake City, UT 84112-0111
(pankow@seis.utah.edu and pechmann@seis.utah.edu)

ABSTRACT

Using data from the Advanced National Seismic System network in and near the Salt Lake Valley (SLV), Utah, we measured average, frequency-dependent, low-strain site-amplification factors for site-response units mapped by others on the basis of geology and near-surface shear-wave velocity. The site-amplification factors were determined using distance-corrected spectral ratios between horizontal-component ground-motion recordings from soil sites and reference rock sites. To test various models for the distance correction terms, we measured spectral ratios between recordings at 12 Paleozoic rock sites. These spectral ratios indicate that the ground motions decrease with hypocentral distance, r, at rates of $r^{-1.5}$ in the period range 0.4 to 2.0 sec and $r^{-2.0}$ in the period range 0.1 to 0.5 sec. We calculated the soil/rock spectral ratios using two different reference stations on Paleozoic rock. Geometric mean site-amplification terms for three SLV site response units were obtained by combining data from both reference stations. Comparing the resultant site-amplification factors to those of previous studies indicates that empirically based predictions better fit the observed data. Specifically, the empirically based site-amplification factors of Borcherdt (1994) and Boore and others (1997) fit the data better than the theoretically based factors of Wong and others (2002a, b), even though the latter were developed specifically for the SLV site-response units.

INTRODUCTION

It has long been recognized that ground motions in sedimentary basins can be greatly affected by soil properties and by the 2- and 3-D basin structure (e.g., Anderson and others, 1986; Singh and others, 1988; U.S. Geological Survey Staff, 1990; Kramer, 1996; Davis and others, 2000; Field and others, 2000; Joyner, 2000). Thus, in characterizing and preparing for earthquake ground shaking in sedimentary basins, an understanding of these properties is a prerequisite. In this paper, we analyze data from the Advanced National Seismic System (ANSS; U. S. Geological Survey, 1999) network in and near the sedimentary basin of the Salt Lake Valley (SLV), Utah, to determine average levels of ground-motion amplification on previously mapped soil site-response units in the basin relative to nearby Paleozoic bedrock sites (Figures 1 and 2).

Earthquake hazards in the SLV are a serious concern because the valley is a major urban center with a population of approximately 900,000 people (40% of the population of Utah). The most obvious source of seismic hazard is the Salt Lake City segment of the Wasatch fault, a major normal fault that separates the Salt Lake Basin from the Wasatch Range to the east (Machette and others, 1991). Paleoseismological studies of the Salt Lake City segment show that large, M~7, surface-faulting earthquakes have occurred on average once every 1,350 ± 200 yrs during the past 6,000 yrs, with the last one occurring 1,230 ± 60 yrs ago (Black and others, 1995; McCalpin and Nishenko, 1996; McCalpin and Nelson, 2000). Based on this information, McCalpin and Nelson (2000) have estimated the probability of such an event occurring during the next 100 years to be about 16%, and Wong and others (2002a) have estimated the probability during the next 50 years to be 6% to 9%. Other active faults located in and near the SLV also

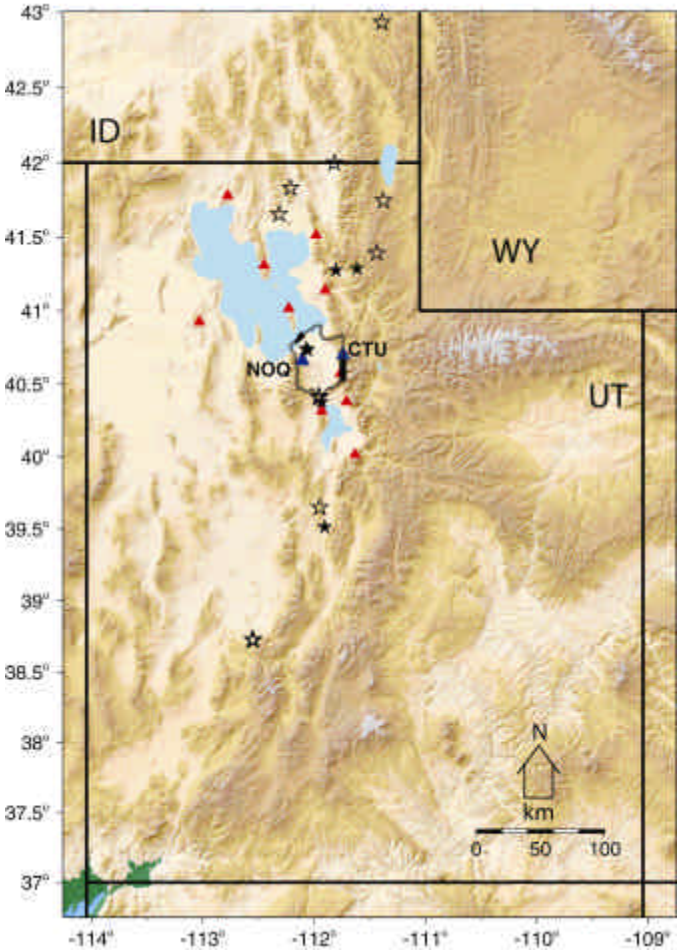

Figure 1. *Map of Utah and the surrounding region showing broadband and strong- motion stations on Paleozoic rock, which we used to test the distance corrections (triangles), the two reference rock stations used to calculate the site-amplification factors (blue triangles), earthquakes used for testing the distance corrections (stars), and earthquakes used to calculate the site-amplification factors (solid stars). The gray polygon outlines the region shown in Figure 2.*

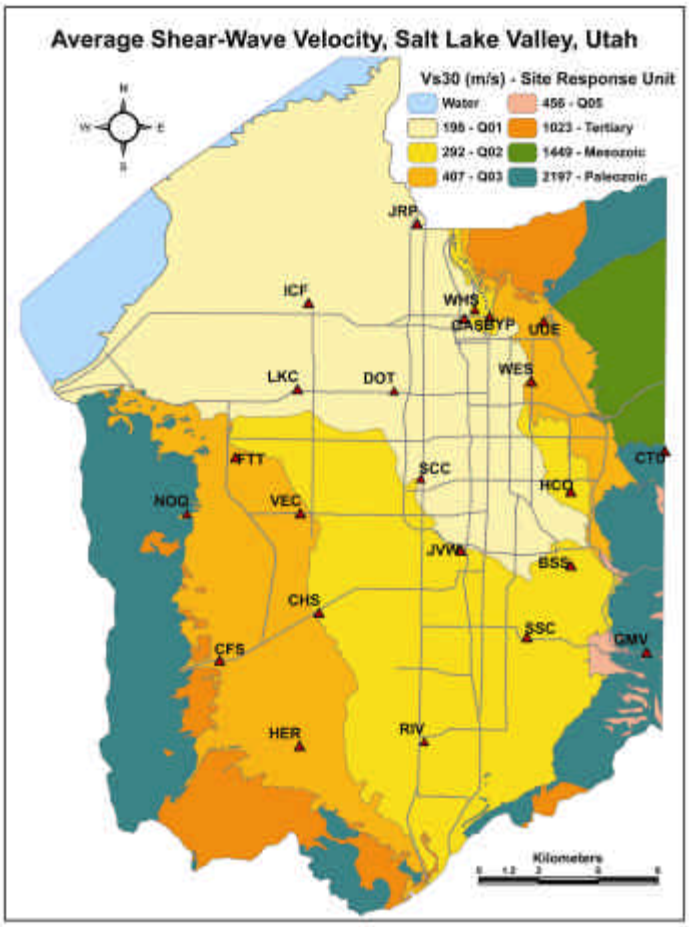

Figure 2. *Map of the Salt Lake Valley, Utah, showing locations of Advanced National Seismic System strong-motion and broadband stations used in this study and geologically based site-response units, which are grouped according to average shear-wave velocity in the uppermost 30 m (Ashland 2001; personal communication 2004).*

pose a significant seismic hazard (Arabasz and others, 1992; Wong and others, 2002a).

Ground-motion amplification in sedimentary basins is commonly characterized by site-amplification factors, which are multiplicative corrections for the effects of "near-surface" materials on ground motions. Site-amplification factors are used extensively in probabilistic and deterministic seismic-hazard analyses and for creating near-real-time maps of ground shaking (ShakeMaps). Site-amplification factors currently used in ground-motion studies are typically functions of both frequency and average shear-wave velocity in the uppermost 30-meters (V_S30). Some of them are also functions of other parameters, such as sediment thickness and the horizontal peak ground acceleration (PGA) of the rock at the base of the sediments.

Site-amplification factors can be grouped into three types based on how they are determined. The first type consists of site-amplification factors that are derived empirically, usually in studies of ground motion predictive relations. A particularly relevant example for Utah is the set of amplification factors determined by Boore and others (1994, 1997), which was subsequently used in the predictive relations for extensional regimes developed by Spudich and others (1999) and

Pankow and Pechmann (2004). The Boore and others (1994, 1997) amplification factors are independent of amplitude and have been used for seismic-hazard analyses in Utah in conjunction with the predictive relations of Boore and others (1994, 1995, 1997) and Spudich and others (1999). The second type of site-amplification factor consists of those which are derived from theoretical methods, such as the well-known equivalent-linear soil response modeling program SHAKE. Examples of such factors include those determined by Wong and others (2002a, b; see also Solomon and others, 2004) for SLV soil site-response units, which they used to create probabilistic and deterministic seismic-hazard maps for the SLV. The Wong and others (2002a, b) site-amplification factors are functions of input rock motion PGA and unconsolidated sediment thickness as well as frequency and V_S30. The third type of site-amplification factor consists of those derived using both empirical and theoretical methods, such as those of Borcherdt (1994). His factors are based on empirical data at low strains and "laboratory and numerical modeling results" at high strains, and are functions of input rock motion PGA, frequency, and V_S30. In Utah, the Borcherdt (1994) amplification factors are used to create ShakeMaps and ShakeMap scenarios (Pankow and others, 2001; Pankow, 2003).

The three different studies cited above predict disparate site-amplification factors for SLV sites at both high and low strain. Even at low strain the differences are large enough that by using weak motion data collected by ANSS instruments throughout the valley, we can select the factors that best fit the weak-motion data. Knowing which, if any, of these sets of site-amplification factors is appropriate for the SLV is crucial for hazard mapping. Use of incorrect site-amplification factors could lead to overestimation or underestimation of predicted ground motions in this area.

In this paper, we apply the spectral-ratio method to weak-motion data collected at ANSS stations to measure frequency-dependent, low-strain site-amplification factors for SLV soil sites. In this method, the ratio between spectra of seismic data from the same event recorded at a soil site and a nearby rock site is interpreted to represent the ground-motion amplification at the soil site relative to the rock site—after applying a distance correction (e.g., Borcherdt, 1970). The measured low-strain site-amplification factors are then averaged over SLV site-response units, which were defined by Ashland (2001 and personal communication, 2004; Figure 2) on the basis of geology and V_S30 measurements, and compared to the three sets of published site-amplification factors discussed above. Although we only have low-strain data, this analysis is important for three reasons. First, at low strain the amplification should be a linear process. If a given set of site-amplification factors cannot predict low-strain, linear amplification then predicted amplifications at higher strain, where non-linear effects are expected, would be questionable. Second, even low-strain site-amplification factors are relevant to seismic-hazard analyses because they are applicable to ground motions up to at least ~0.15 g (Borcherdt, 1994; Beresnev and Wen, 1996; Wong and others, 2002a), and the threshold of damage to weak construction is about 0.1 g (Richter, 1958, p. 26). Finally, our study in the linear soil-response domain will provide a baseline for studying non-linear effects when future large earthquakes occur in the SLV.

DATA

Eighteen local earthquakes recorded at ANSS strong-motion and broadband stations make up the dataset for this study (Table 1 and Figure 1). These earthquakes range in local magnitude (M_L) from 2.0 to 5.3 and are at epicentral distances of 10 to 260 km from the primary rock reference station, NOQ (see Figure 2). All 18 events were used to test possible distance correction methods for the spectral ratios. Six events that were well-recorded by stations located on soil in the SLV were used to determine site amplification. The epicentral distances from these six events to the soil sites used to determine site-amplification factors range from

Table 1. ***Earthquakes used in this study†***

DATE (YEAR MO DY)	ORIGIN TIME (UTC)	LATITUDE	LONGITUDE	DEPTH (KM)	MAG. (M_L)	DIST TO NOQ (KM)
20010223	21:43:50.82	38.7270°	-112.555°	1.10	4.0	217
20010224	10:54:40.75	38.7265°	-112.544°	2.02	3.6	217
20010228	04:09:46.14	38.7217°	-112.546°	0.16	3.6	218
20010421	17:18:56.28	42.9320°	-111.391°	1.04	5.3	260
20010524*	02:40:40.89	40.3762°	-111.933°	6.44	3.3	35
20010708*	13:55:51.33	40.7418°	-112.073°	10.81	3.3	11
20020614	07:45:46.38	41.3917°	-111.436°	7.39	3.0	100
20020728	19:38:40.03	41.7453°	-111.379°	9.39	3.6	136
20020921	20:14:15.02	40.4177°	-111.958°	11.53	2.7	29
20021004	12:30:56.98	41.6548°	-112.312°	0.06	2.4	112
20021010	06:52:43.82	40.4073°	-111.953°	6.34	2.0	31
20030103*	05:02:12.16	41.2747°	-111.802°	11.86	3.6	74
20030201	20:37:31.24	41.8285°	-112.212°	0.17	3.2	131
20030417*	01:04:19.07	39.5130°	-111.905°	0.88	4.3	128
20030712*	01:54:40.04	41.2857°	-111.615°	9.23	3.5	82
20031227	00:39:24.37	39.6485°	-111.950°	1.85	3.6	112
20040225	00:41:03.64	41.9970°	-111.818°	2.46	3.4	151
20040318*	21:22:37.49	40.7302°	-112.056°	7.93	2.4	10

† locations and magnitudes are from the University of Utah earthquake catalog (http://www.quake.utah.edu)
** denotes events used to calculate soil/rock spectral-amplitude ratios; all events were used to evaluate the distance corrections*

2 to 146 km, with a median of 60 km. The earthquakes occurred both north and south of the valley, providing some azimuthal variation in the ray paths (Figure1). There were also two events located beneath the valley itself.

The dataset used for the distance correction tests was recorded at 12 stations located on Paleozoic rock in northern Utah (Figure 1). We selected this group of stations in order to obtain a widespread distribution with minimal differences in site response. We calculated the site-amplification factors using 20 stations located on soil and two reference rock stations located on Paleozoic rock near the SLV: NOQ and CTU. NOQ is west of the valley on Permian limestone. CTU is east of the valley on Pennsylvanian quartzite. Seismic refraction data indicate that the near-surface *P*-wave velocity of the quartzite is 1745 m/sec (G. T. Schuster, written communication, 1993) which, assuming a near-surface *P*-to-*S* velocity ratio of 2.0, suggests an S-wave velocity of ~870 m/sec. Both reference stations have GURALP broadband velocity sensors and REF-TEK digital recorders operating at sample rates of 100 samples/sec. The soil sites where amplification factors were measured are well-distributed throughout the valley on the three main V_S30 units (Figure 2). The instruments at these sites are either Kinemetrics Model K2 recorders with episensor accelerometers or REF-TEK Model ANSS-130 recorders with MEMS accelerometers. These data are also recorded digitally at 100 samples/sec.

METHODOLOGY

Interpretation of Spectral Ratios

The theoretical basis of the spectral-ratio method is the following simple, but widely used, frequency-domain model for ground motion:

$$A_{ij}(r_{ij}, f) = E_i(r_{ref}, f)\, S_j(f)\, D(r_{ref}, r_{ij}, f) \qquad (1)$$

where A_{ij} is the spectral amplitude of ground motion from earthquake i recorded at station j, r_{ij} is the hypocentral distance from earthquake i to station j, f is frequency, $E_i(r_{ref}, f)$ is a source excitation term, assumed to be isotropic, which gives the spectral amplitude of ground motion from earthquake i at reference distance r_{ref}, $S_j(f)$ is the site-amplification factor, and $D(r_{ref}, r_{ij}, f)$ is a function describing the distance dependence of the ground motion. To the extent that the assumption of an isotropic source is valid, the source term can be removed by computing the ratio between the spectral amplitudes of ground motion from the same earthquake recorded at two stations, station j and reference station o. Computing this ratio and solving for the ratio of the site-amplification factors for the two stations gives

$$\frac{S_j(f)}{S_o(f)} = \frac{A_{ij}(r_{ij}, f)\, D(r_{ref}, r_{io}, f)}{A_{io}(r_{io}, f)\, D(r_{ref}, r_{ij}, f)} \quad . \qquad (2)$$

Thus, the site-amplification factor of station j relative to that of reference station o, $S_j(f)/S_o(f)$, can be determined from the observed spectral ratio, $A_{ij}(r_{ij}, f)/A_{io}(r_{io}, f)$, provided that the distance correction $D(r_{ref}, r_{io}, f)/ D(r_{ref}, r_{ij}, f)$ is known.

Data Processing

We applied the following processing procedure to all of the raw waveform data for this study to obtain velocity traces in the passband 0.4 to 40 Hz: (1) removal of the DC offset, (2) tapering with a 5% Hanning taper, (3) deconvolution of the instrument velocity response by spectral division, and (4) highpass filtering with a frequency domain cosine taper between 0.2 and 0.4 Hz. We then calculated the Fourier spectra of both horizontal components for a 50-sec data window beginning 5 seconds before the *P*-wave arrival and for a 25-sec noise window immediately prior to the *P*-wave window. Before computing the spectra, a 10% Hanning taper was applied to the windows and they were padded with zeros to twice their original length. Finally, we computed average horizontal spectral ratios over the mid-period (0.5 to 2.5 Hz) and short-period (2 to 10 Hz) bands of Borcherdt (1994), using only records for which the spectral signal-to-noise ratio was greater than 3 over the entire band. For the purposes of this study, the average horizontal spectral ratio is defined as

$$\frac{A_{ij}(r_{ij}, f)}{A_{io}(r_{io}, f)} = \frac{A_{ijE}(f) + A_{ijN}(f)}{A_{ioE}(f) + A_{ioN}(f)} \quad . \qquad (3)$$

where $A_{ijE}(f)$ and $A_{ijN}(f)$ are the Fourier amplitude spectra of earthquake i recorded on the east and north components, respectively, of station j. The spectrum of each component was smoothed separately with a moving average of ± 16 points (± 0.1 Hz) before computing the spectral ratio. Figures 3 and 4 show examples of processed data in the time and frequency domains, respectively.

Distance Corrections

The distance function D in (1) is generally assumed to have the form

$$D(r_{ref}, r_{ij}, f) = \frac{g(r_{ij})}{g(r_{ref})} e^{-p\, f\, (r_{ij} - r_{ref}) / b\, Q(f)} \qquad (4)$$

where $g(r_{ij})$ is the geometrical spreading function, β is the average shear-wave velocity along the raypaths, and $Q(f)$ is a frequency-dependent quality factor $Q_o f^{\eta}$, where Q_o and η are constants. From (4), the distance correction factor in (2) takes the form

$$\frac{D(r_{ref}, r_{io}, f)}{D(r_{ref}, r_{ij}, f)} = \frac{g(r_{io})}{g(r_{ij})} e^{-p\, f\, (r_{io} - r_{ij}) / b\, Q(f)} \qquad (5)$$

which is independent of r_{ref} (e.g., Hartzell and others, 1996; Harmsen, 1997).

Brockman and Bollinger (1992) and Jeon and Herrmann (in press) have modeled the distance dependence of S_g/L_g ground motion spectral

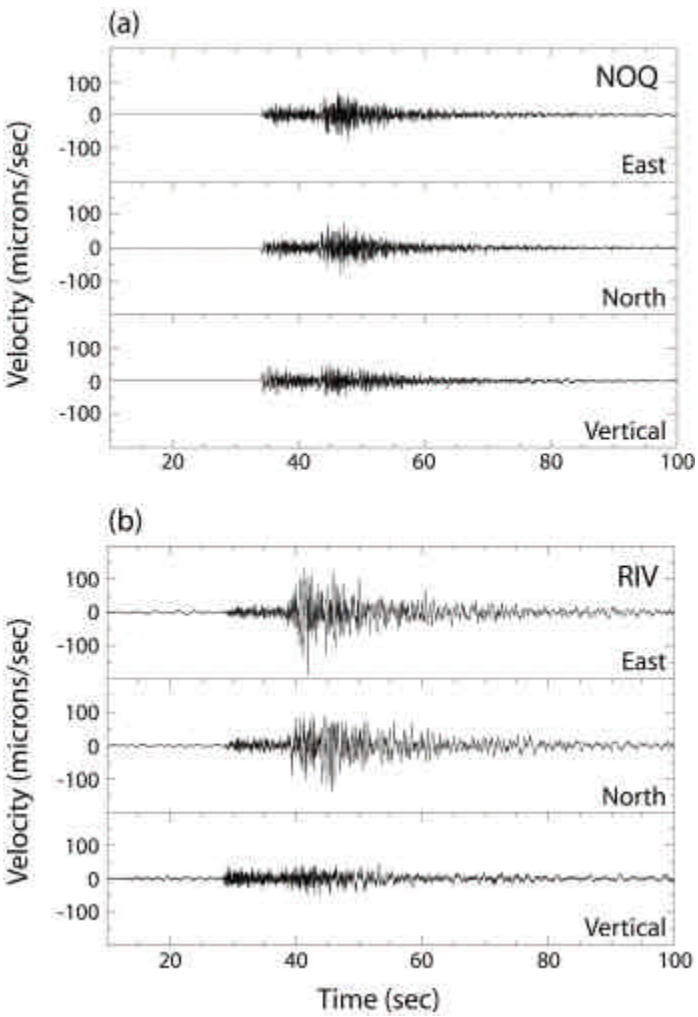

Figure 3. *Velocity records (filter bandpass 0.4 – 40 Hz) from the soil site RIV (hypocentral distance 85.5 km) and the rock reference station NOQ (hypocentral distance 75.0 km) for an ML 3.6 earthquake on Jan. 3, 2003.*

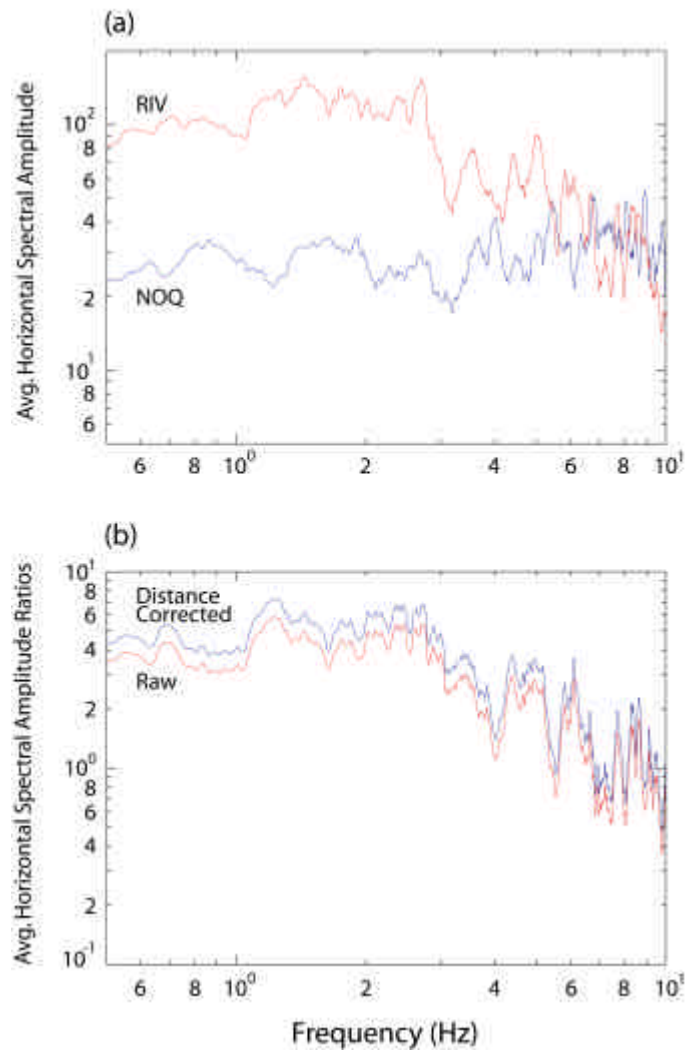

Figure 4. *(a) Average horizontal-component spectra for the velocity records in Figure 3: NOQ (blue) and RIV (red). (b) The average horizontal component spectral-amplitude ratios—distance corrected (blue) and uncorrected (red)—for the two stations in (a).*

amplitudes in Utah by inverting for the parameters in (1) and (4) using data from the Utah regional seismic network. In order to test the accuracy of spectral ratio distance corrections based on their models and another model discussed below, we used records of 18 local earthquakes from 12 northern Utah stations located on Paleozoic rock—including the two stations which we selected as reference rock stations for our study (Figure 1, Table 1). We calculated ratios between average horizontal-component Fourier spectra of the records from all of the possible pairs of stations which recorded each earthquake. For these spectral ratios, if it is assumed that all of the Paleozoic rock sites have similar site-amplification factors, then $S_j(f)/S_o(f) \approx 1$ and (2) simplifies to

$$\frac{A_{ij}(r_{ij}, f)}{A_{io}(r_{io}, f)} = \frac{D(r_{ref}, r_{ij}, f)}{D(r_{ref}, r_{io}, f)} \quad . \qquad (6)$$

Thus, with this data set, the accuracy of the distance corrections can be evaluated by comparing the observed and predicted spectral ratios on the left - and right-hand sides of equation (6), respectively. We made such comparisons using average values of

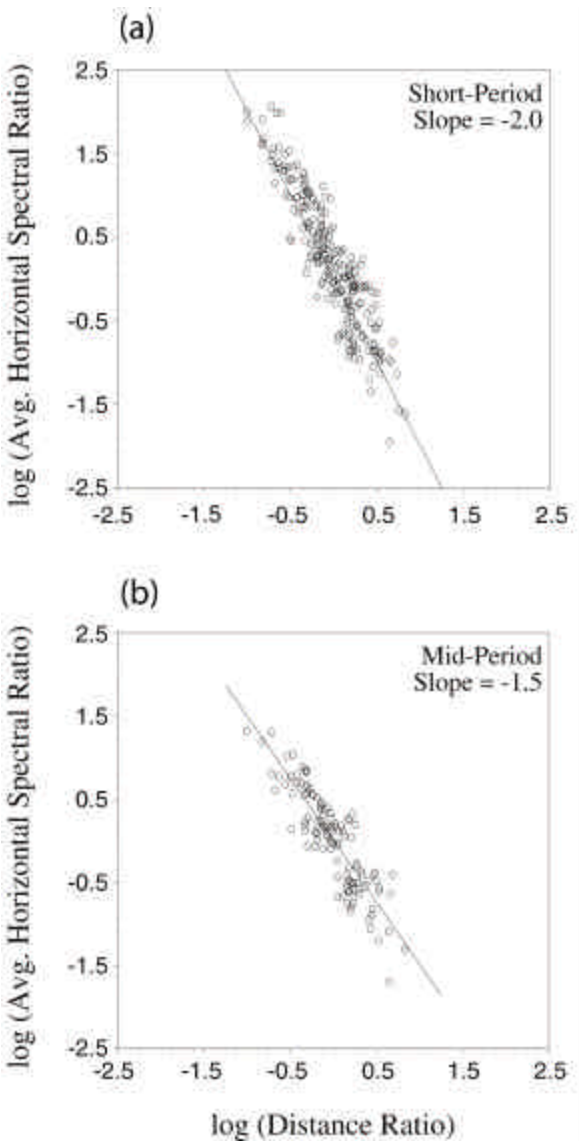

Figure 5. *Observed spectral ratios plotted versus $\log_{10}$(Distance Ratio), where the distance ratio is the ratio between the hypocentral distances of the two stations. (a) short-period band (0.1 to 0.5 sec) and (b) mid-period band (0.4 to 2.0 sec). The lines indicate fits to the data for an exponential model (see text).*

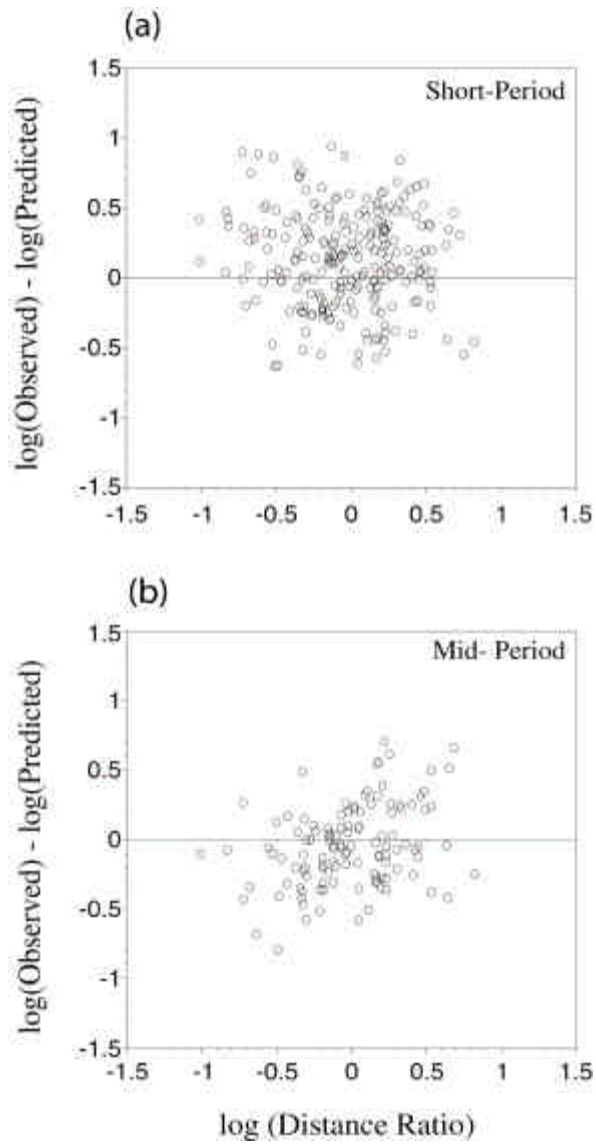

Figure 6. *Spectral-ratio residuals, defined as $\log_{10}$ (Observed Ratio) - $\log_{10}$ (Predicted Ratio), versus $\log_{10}$ (Distance Ratio), where the distance ratio is the ratio between the hypocentral distances of the two stations. The observed ratios are between average horizontal-component Fourier amplitude spectra of recordings from the same event at two different Paleozoic rock sites (see Figure 1), averaged over the short-period band (0.1 to 0.5 sec) in (a) and the mid-period band (0.4 to 2.0 sec) in (b). The predicted ratios are based on the Brockman and Bollinger (1992) model for Sg/Lg geometrical spreading and attenuation in Utah, and assume that the effects of site amplification and the source are similar at both recording sites. The plots demonstrate that there is no significant bias in the spectral-ratio residuals.*

the observed spectral ratios over the mid-period (0.5 to 2.5 Hz) and short-period (2 to 10 Hz) bands. The predicted values were calculated for the frequencies at the mid points of these period bands: 1.5 and 6.0 Hz, respectively.

Figure 5 shows the logarithms of the observed spectral ratios plotted versus $\log_{10}(r_{ij}/r_{io})$. The lines on the plots show linear regression fits to the data for the simple exponential model

$$\frac{A_{ij}(r_{ij}, f)}{A_{io}(r_{io}, f)} = \left(\frac{r_{ij}}{r_{io}}\right)^{-p} . \qquad (7)$$

where p is a constant. The best-fit p values and their 95% confidence limits are 1.5 ± 0.2 and 2.0 ± 0.1 for the mid-period and short-period bands, respectively. It is worth noting that both of these p values are much higher than 1.0, the value which is often assumed for exponential distance-correction functions based on geometrical spreading for body waves in a homogeneous half space (e.g., Borcherdt and Glasmoyer, 1992; Borcherdt, 1994).

Overall, the Brockman and Bollinger (1992) model provides a better fit to the data in Figure 5 than the exponential model shown on this figure or the Jeon and Herrman (in press) model. Figure 6 shows plots of spectral ratio residuals,

$$\log_{10}(Observed) - \log_{10}(Predicted) =$$

$$\log_{10}\frac{A_{ij}(r_{ij}, f)}{A_{io}(r_{io}, f)} - \log_{10}\frac{D(r_{ref}, r_{ij}, f)}{D(r_{ref}, r_{io}, f)} \quad (8)$$

versus $\log_{10}(r_{ij}/r_{io})$ for the Brockman and Bollinger (1992) model. These plots and similar plots versus r_{io} show that there is no significant distance bias in the spectral ratio residuals, although the mid-period residuals show a slight tendency to increase with the distance ratio r_{ij}/r_{io}. It is surprising that the Brockman and Bollinger (1992) model fits our horizontal-component spectral ratios better than the Jeon and Herrmann (in press) model. The data set for the former study was five times smaller and consisted of vertical-component records only, whereas Jeon and Herrmann used both horizontal- and vertical-component data. However, Jeon and Herrmann did not find much difference in the distance dependence of ground motion spectral amplitudes on horizontal and vertical components and recommended a single model for both components. Based on our tests, we decided to correct our soil/rock spectral ratios at each frequency point using equation (5) with the parameters from the Brockman and Bollinger (1992) model: $g(r_{ij}) = r_{ij}^{-0.9}$, b = 3.5 km/sec, and $Q(f) = 97f^{0.80 \pm 0.08}$.

Determination of Average Site-Amplification Factors

To obtain the best possible estimate of the average site-amplification factors for each SLV site-response unit, we calculated the geometric mean of the distance-corrected spectral ratios for all of the stations located on that unit. Initially, these geometric means were calculated separately for the spectral ratios relative to each of the two reference rock sites, NOQ and CTU (Figure 2). It is desirable to combine the spectral ratios for both reference rock sites because of the limited amount of data and the need to average out source effects. However, NOQ/CTU spectral ratios indicate that ground motions at NOQ are amplified significantly relative to those at CTU, with average geometric mean amplification factors of 1.45 and 1.93 for the mid-period and short-period bands, respectively (Figure 7c). Therefore, it is necessary to correct the soil/rock spectral ratios for the differences in site amplification at the two reference rock sites. We chose to adjust the geometric mean CTU-referenced spectral ratios to NOQ site conditions and then compute the geometric mean of this result and the geometric mean NOQ-referenced spectral ratios. Let $\bar{S}_{k/NOQ}(f)$ and $\bar{S}_{k/CTU}(f)$ be the geometric means of the distance-corrected spectral ratios for stations on site-response unit k relative to NOQ and CTU, respectively. Let $\bar{S}_{NOQ/CTU}(f)$ be the geometric mean of the distance-corrected spectral ratios for NOQ relative to CTU. Finally, let $\bar{S}_k(f)$ be the combined NOQ-CTU geometric mean of the distance-corrected spectral ratios for stations on site-response unit k, relative to NOQ rock site conditions. $\bar{S}_k(f)$, as defined by the equation

$$\log \bar{S}_k(f) = \frac{1}{2}\left[\log \bar{S}_{k/NOQ}(f) + \log(\bar{S}_{k/CTU} / \bar{S}_{NOQ/CTU})\right] \quad (9)$$

is our preferred estimate of the average site-amplification factors for site-response unit k. Note

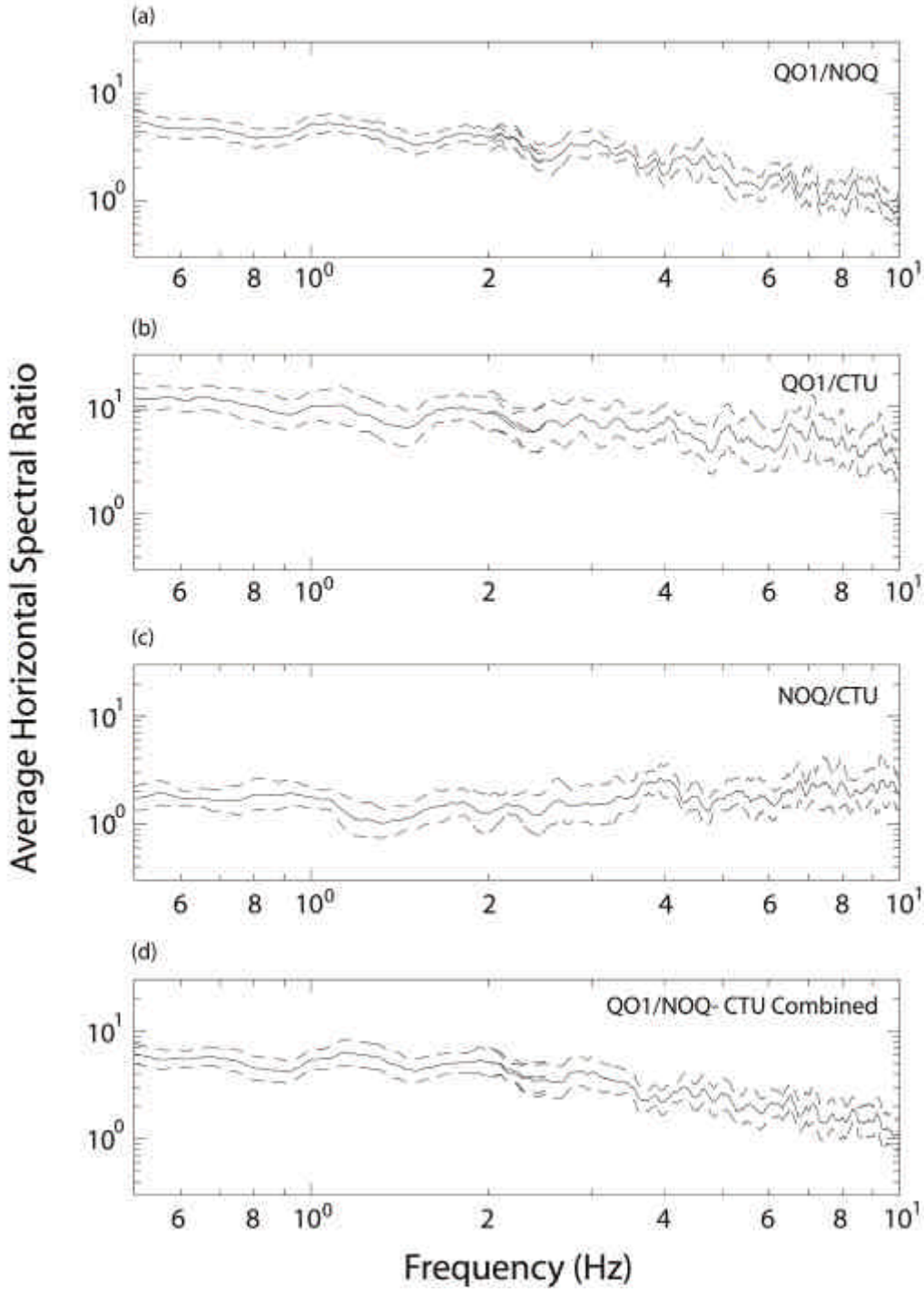

Figure 7. *Steps involved in calculating the average site-amplification factors for site-response unit Q01. The geometric means (solid lines) of the distance-corrected spectral ratios for stations on site-response unit Q01 relative to NOQ [(a);* $\overline{S}_{k/NOQ}(f)$ *] and CTU [(b);* $\overline{S}_{k/CTU}(f)$ *]. (c) The distance-corrected spectral ratios for station NOQ relative to CTU [* $\overline{S}_{NOQ/CTU}(f)$ *]. (d) The combined NOQ-CTU geometric mean of the distance-corrected spectral ratios for stations on site-response unit Q01 relative to NOQ rock site conditions,* $\overline{S}_k(f)$*. The dashed lines show the 95% confidence limits on the geometric means.*

that $\bar{S}_{k/NOQ}(f)$ and $\bar{S}_{k/CTU}(f)$ are given equal weight in calculating $\bar{S}_k(f)$. Weighting $\bar{S}_{k/NOQ}(f)$ and $\bar{S}_{k/CTU}(f)$ by the number of spectral ratios used to determine each would not have a large effect on the result because the numbers of spectral ratios relative to NOQ and CTU are comparable. If the 95% confidence limits on $\log\bar{S}_{k/NOQ}(f)$, $\log\bar{S}_{k/CTU}(f)$, and $\log\bar{S}_{NOQ/CTU}(f)$ are designated by $2s\,(\log\bar{S}_{k/NOQ}(f))$, $2s\,(\log\bar{S}_{k/CTU}(f))$, and $2s\,(\log\bar{S}_{NOQ/CTU}(f))$, respectively, then if we assume that all three of these quantities can be treated as independent random variables, the 95% confidence limits on $\log\bar{S}_k(f)$ are given by

$$2s\,(\log\bar{S}_k(f)) = \frac{1}{2}\Big[\big(2s\,(\log\bar{S}_{k/NOQ}(f))\big)^2 + \big(2s\,(\log(\bar{S}_{k/CTU}(f))\big)^2 + \big(2s\,(\log\bar{S}_{NOQ/CTU}(f))\big)^2\Big]^{1/2} \quad (10)$$

To illustrate the steps involved in calculating the average site-amplification factors, Figure 7 shows $\bar{S}_{k/NOQ}(f)$, $\bar{S}_{k/CTU}(f)$, $\bar{S}_{NOQ/CTU}(f)$, and $\bar{S}_k(f)$ for site-response unit Q01. Note that the data sets for the mid-period (0.5 to 2.5 Hz) and short-period (2 to 10 Hz) bands are not exactly the same because some records had adequate signal-to-noise ratios in only one of these two bands. Nevertheless, the two sets of functions agree very well in the frequency range 2.0 to 2.5 Hz where the mid-period and short-period bands overlap.

RESULTS

Figure 8 shows the combined geometric mean spectral ratios relative to reference station NOQ for the three largest V_S30 units in the SLV (Figure 2). The geometric mean spectral ratio for site-response unit Q01 is significantly higher than that of Q03 over nearly the entire frequency range examined, 0.5 to 10 Hz. The geometric mean spectral ratios for Q02 generally lie between those of Q01 and Q03 for the frequency range of 0.5 to 4 Hz and are comparable to those of Q03 at higher frequencies. The 95% confidence limits for Q02 and Q03 overlap over the whole frequency range shown. Relative to NOQ rock-site conditions, we find mean mid-period amplification factors ranging from 2.1 on Q03 to 4.9 on Q01 and mean short-period amplification factors ranging from 1.1 on Q03 to 2.3 on Q01 (Table 2).

Figure 9 shows the comparison of our results with the three previously mentioned sets of site-amplification factors, which can be used to predict ground motion differences among the SLV site-response units. Wong and others (2002a, b) calculated their site-amplification factors relative to ground motions at the surface of a generic western U.S. soft rock profile for which we computed a V_S30 of 530 m/s. We calculated the site-amplification factors of Borcherdt (1994) and Boore and others (1997) shown in Figure 9 assuming a reference rock V_S30 of 910 m/sec (Pankow and Pechmann, 2004)—similar to our estimate of the near-surface shear-wave velocity at reference station CTU (~870 m/sec). If we had used a reference V_S30 of 530 m/sec instead of 910 m/sec for our calculations, then on Figure 9 these two sets of amplification factors would be ~20% lower in the short-period band and ~30% lower in the mid-period band.

For Q01 we observe higher amplification factors than predicted by any of the three models. For Q02 and Q03 the data more closely match the predictions of Borcherdt (1994) and Boore and others (1997), than those of Wong and others (2002a, b). The observed mid-period site-amplification factors are higher than the observed short-period amplification factors for all three site-response units. The empirically based amplification factors of Boore and others (1997) and Borcherdt (1994) are also higher in the mid-period band than in the short-period band, but the differences are smaller than we observe.

We observe, consistent with the predictions

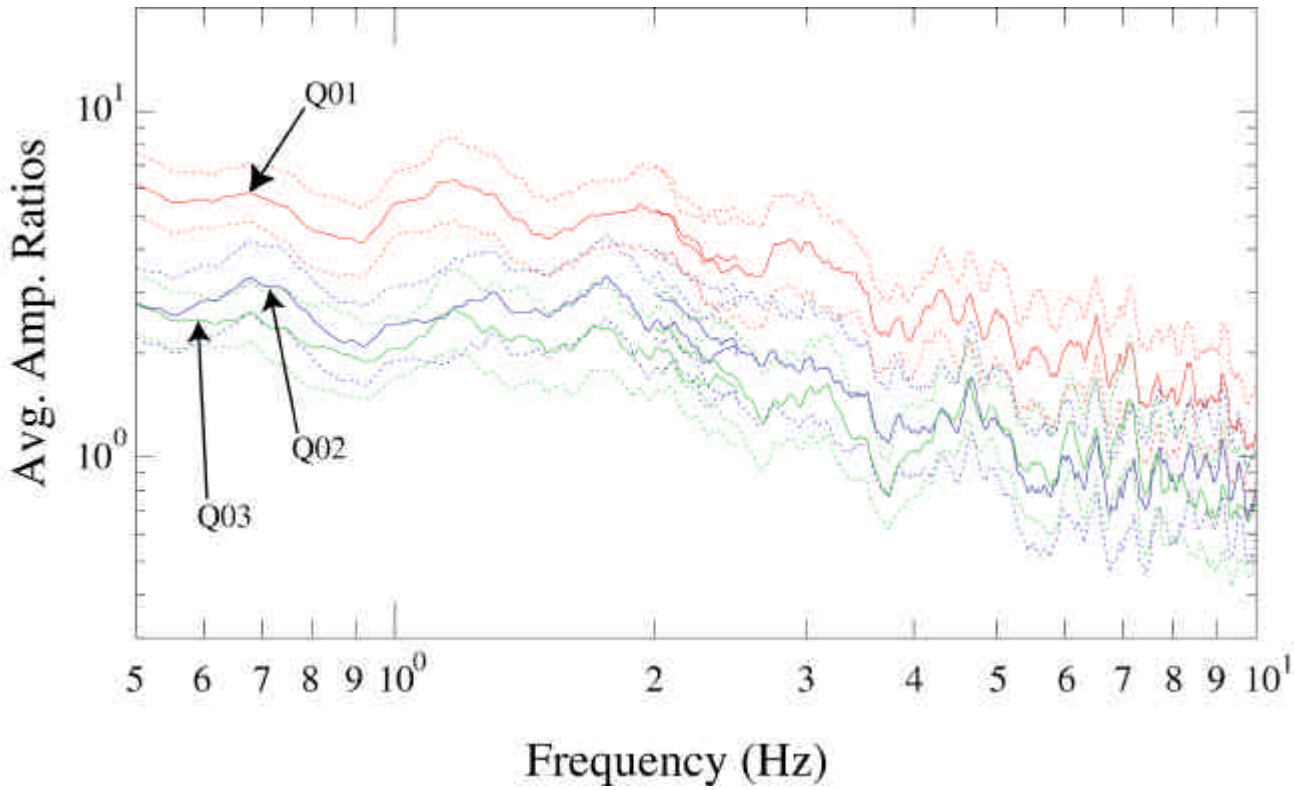

Figure 8. *Combined NOQ-CTU spectral ratios relative to station NOQ (Figure 2) over the frequency range 0.5 to 10.0 Hz for three different SLV site-response units (Figure 2): Q01 (red), Q02 (blue), and Q03 (green). Shown are the geometric mean spectral ratios (solid lines) and their 95% confidence limits (dotted lines).*

TABLE 2. ***Empirical low-strain site-amplification factors****

SALT LAKE VALLEY SITE-RESPONSE UNIT	SHORT-PERIOD FACTOR 0.1-0.5 SEC	MID-PERIOD FACTOR 0.4-2.0 SEC
Q01—Lacustrine and alluvial silt, clay, and fine sand	2.27 (3.08, 1.67)	4.92 (6.28, 3.85)
Q02—Lacustrine sand and gravel; interbedded lacustrine silt, clay, and sand	1.18 (1.68, 0.831)	2.57 (3.39, 1.96)
Q03—Lacustrine and alluvial gravel and sand	1.10 (1.51, 0.800)	2.12 (2.76, 1.63)

**Values in parentheses are upper- and lower-bound 95% confidence limits*

of Borcherdt (1994) and Boore and others (1997), that the short-period amplification factors are higher on the deep soft soils of Q01 than on the thin stiff soils of Q03. This result disagrees with the predictions of Wong and others (2002a, b), which show lower short-period site-amplification factors on Q01 than on Q03. The theoretical amplification factors of Wong and others (2002a, b), which depend on sediment thickness, show a general increase in amplification factors with increasing period from 0.1 to between 0.4 and 0.8 sec.

However, at ~0.6 sec the site-amplification factors begin to decrease with period. The decrease is more pronounced for shallow sediment thickness than for the deeper columns of sediment. We do not observe this decrease in our data.

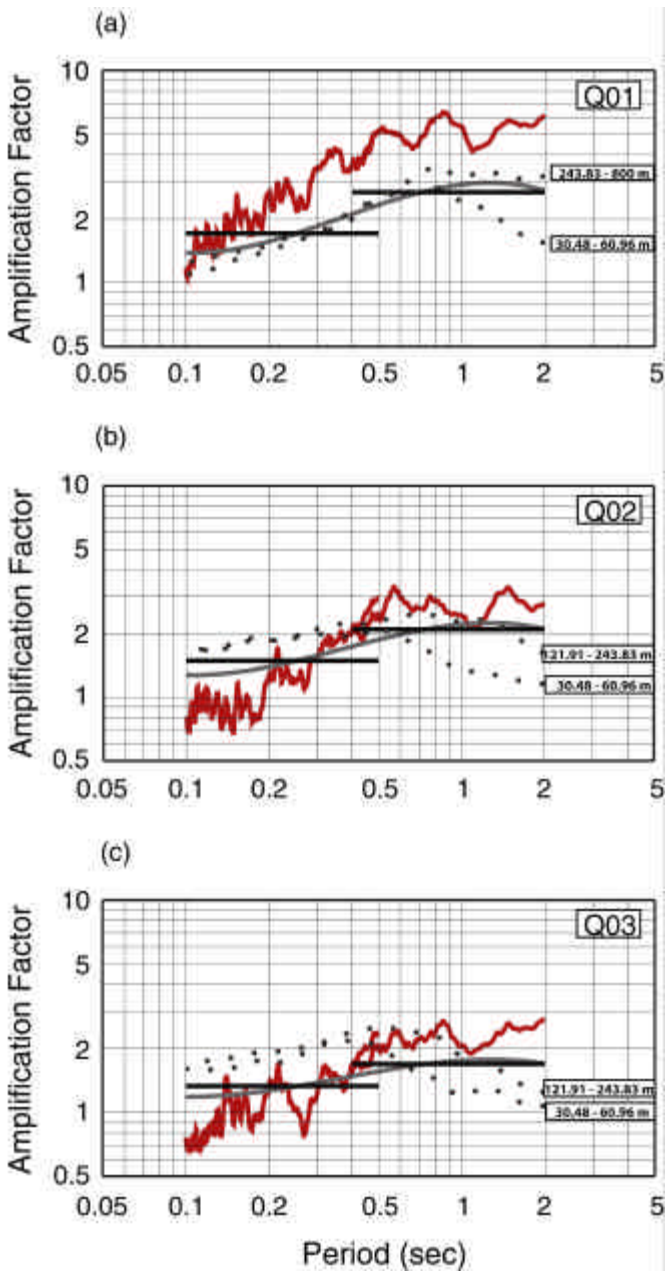

Figure 9. *Observed (red) and predicted (black and gray) site-amplification factors as a function of period for three different SLV site-response units. The observed amplification factors are geometric means (solid red lines) from this study, relative to NOQ site conditions. The predicted amplification factors from Borcherdt (1994, solid black lines), for rock peak acceleration 0.1 g, and Boore and others (1997, solid gray lines) were calculated assuming a reference rock site V_S30 of 910 m/sec (Pankow and Pechmann, 2004). The predicted amplification factors from Wong and others (2002a, b; dotted black lines), for rock peak acceleration of 0.05 g, are shown for two different ranges of unconsolidated sediment depth as labeled on the plots. (a) Q01, (b) Q02, and (c) Q03.*

CONCLUSIONS

In this study, we set out to determine if any of three sets of site-amplification factors, which have been applied to the SLV, match observed low-strain data. Overall, the data for the three most widespread V_S30 units in the SLV (Figure 2) are best matched by the site-amplification factors of Borcherdt (1994) and Boore and others (1997). However, their predicted amplification factors show less variability with period and with V_S30 unit than we observe (Figure 9). One limitation of our study is that we do not have the data to fully account for sediment thickness as was done in Wong and others (2000a, b), and thus our site-amplification factors are averaged values. However, the ranges of sediment thickness plotted for Wong and others (2002a, b) on Figure 9 span the thickness ranges of Arnow and others (1970) for each unit in the SLV. If the site-amplification factors of Wong and others (2000a, b) are correct, we would expect the general shapes of the curves to mimic those of the measured amplification factors. But this is not the case. The Wong and others (2002a, b) factors show decreases in site amplification at periods above ~0.6 sec. This decrease is not observed in our geometrical mean site-amplification factors, nor was it observed in the processing of the individual spectral ratios. Given this discrepancy, the unknowns associated with sediment thickness, and the higher short-period amplification factors on the thin stiff soil (Q03) compared to the thick soft soil (Q01) incorrectly predicted by Wong and others (2002a, b), we conclude that, at least with the present state of knowledge, the empirically based site-amplification factors of Borcherdt (1994) and Boore and others (1997) provide the best alternatives for estimating site amplification in the SLV.

ACKNOWLEGMENTS

We are grateful to Ivan Wong for providing digital files of the Wong and others (2002a, b) reference rock model and site-amplification factors

and to Francis Ashland for providing the revised Salt Lake Valley site-response unit map. Constructive reviews by Relu Burlacu, Walter Arabasz, and editor Bill Lund led to improvements of this article. This research was supported by the U. S. Geological Survey, Department of the Interior, under USGS Award Number 03HQGR0134.

REFERENCES

Anderson, J.G., Bodin, P., Brune, J.N., Prince, J., Singh, S.K., Quaas, R. and Onate, M., 1986, Strong ground motion from the Michoacan, Mexico, earthquake: Science, v. 233, p. 1043-1049.

Arnow, T., Van Horn, R., and LaPray, R., 1970, The pre-Quaternary surface in the Jordan Valley, Utah: U.S. Geological Survey Professional Paper. 700-D, p. D257-D261.

Arabasz, W.J., Pechmann, J.C., and Brown, E.D., 1992, Observational seismology and the evaluation of earthquake hazards and risk in the Wasatch front area, Utah, *in* Gori, P.L. and Hays W.W., editors, Assessment of Regional Earthquake Hazards and Risk Along the Wasatch Front, Utah: U.S. Geological Survey Professional Paper. 1500-A-J, D1-D36.

Ashland, F.X., 2001, Site-response characterization for implementing SHAKEMAP in northern Utah. Utah Geological Survey Report of Investigation 248, 10 p., 2 pl.

Beresnev, I.A., and Wen, K.L., 1996, Nonlinear soil response; a reality?: Bulletin of the Seismological Society of America, v 86, p. 1964-1978.

Black, B.D., Lund, W.R., and Mayes, B.H., 1995, Large earthquakes on the Salt Lake City segment of the Wasatch fault zone-summary of new information from the South Fork Dry Creek site, Salt Lake County, Utah, *in* Lund, W.R., editor, Environmental and Engineering Geology of the Wasatch Front Region: 1995 Symposium and Field Conference, Utah Geological Association Publication, v. 24, p. 11-30.

Boore, D.M., Joyner, W.B., and Fumal, T.E., 1994, Estimation of response spectra and peak accelerations from western North American earthquakes: An interim report, Part 2: U.S. Geological Survey, Open-File Report. 94-127, 40 p.

Boore, D.M., Joyner, W.B., and Fumal, T.E., 1995, Ground motion estimates for strike- and reverse-slip faults: Letter to colleagues, 4 p.

Boore, D.M., Joyner, W.B., and Fumal, T.E., 1997. Equations for estimating horizontal response spectra and peak acceleration from western North American earthquakes: A summary of recent work: Seismological Research Letters. v. 68, p. 128-153.

Borcherdt, R.D, 1970, Effects of local geology on ground motion near San Francisco Bay: Bulletin of the Seismological Society of America, v. 60, p. 29-61.

Borcherdt, R. D., 1994, Estimates of site-dependent response spectra for design (methodology and justification): Earthquake Spectra, v. 10, p. 617-653.

Borcherdt, R. D., and Glassmoyer, G., 1992, On the characteristics of local geology and their influence on ground motions generated by the Loma Prieta earthquake in the San Francisco Bay region, California: Bulletin of the Seismological Society of America, v. 82, p. 603-641.

Brockman, S. R., and Bollinger, G. A., 1992, Q estimates along the Wasatch Front in Utah derived from Sg and Lg wave amplitudes: Bulletin of the Seismological Society of America, v. 82, p. 135-147.

Davis, P.M., Rubinstein, J.L., Liu, K.H., Gao, S.S., and Knopoff, L., 2000, Northridge earthquake damage caused by geologic focusing of seismic waves: Science, v. 289, p. 1746-1750.

Field, E.H., and the SCEC Phase III Working Group, 2000. Accounting for site effects in probabilistic seismic hazard analyses of southern California: Overview of the SCEC Phase III report: Bulletin of the Seismological Society of America, v. 90, p. S1-S31.

Hartzell, S. H, Leeds, A., Frankel, A. D., and

Michael, J. A., 1996, Site response for urban Los Angeles using aftershocks of the Northridge earthquake: Bulletin of the Seismological Society of America, v.86, Part B Suppl., p.S168-S192.

Harmsen, S. C., 1997, Estimating the diminution of shear-wave amplitude with distance; application to the Los Angeles, California, urban area: Bulletin of the Seismological Society of America, v.87, p.888-903.

Jeon, Y., and Hermann, R. B., in press, High frequency earthquake ground motion scaling in Utah and Yellowstone: Bulletin of the Seismological Society of America.

Joyner, W.B., 2000, Strong motion from surface waves in deep sedimentary basins: Bulletin of the Seismological Society of America, v. 90, p. S95-S112.

Kramer, S.L., 1996, Geotechnical earthquake engineering: Upper Saddle River, New Jersey, Prentice Hall, 653 p.

Machette, M.N., Personius, S.F., Nelson, A.R., Schwartz, D.P., and Lund, W.R., 1991, The Wasatch fault zone, Utah-segmentation and history of Holocene earthquakes: Journal of Structural Geology, v. 13, p. 137-149.

McCalpin, J.P., and Nishenko, S.P., 1996, Holocene paleoseismicity, temporal clustering, and probabilities of future large (M > 7) earthquakes on the Wasatch fault zone, Utah: Journal of Geophysical Research, v. 101, p. 6233-6253.

McCalpin, J.P. and Nelson, C.V., 2000, Long recurrence records from the Wasatch fault zone, Utah: Final Technical Report, Contract 99HQGR0058, National Earthquake Hazards Reduction Program, U.S. Geological Survey, 61 p.

Pankow, K. L., Pechmann, J. C., Nava, S. J., and Arabasz, W. J., 2001, Implementing ShakeMap in Utah before the 2002 Winter Olympics: Seismological Research Letters, v. 72, pp. 232.

Pankow, K.L., 2003, The anatomy of an earthquake scenario: M7 on the Salt Lake City segment of the Wasatch fault, Utah: Geophysical Research Abstracts 5, EGS-AGU-EUG Joint Assembly, Compact Disk, ISSN No. 1029-7006.

Pankow, K. L., and Pechmann, J. C., 2004, The SEA99 ground-motion predictive relations for extensional tectonic regimes: Revisions and a new peak ground velocity relation: Bulletin of the Seismological Society of America, v. 94, p. 341-348.

Richter, C.F., 1958, Elementary seismology: San Francisco, CA, W.H. Freeman and Co., 768 p.

Solomon, B.J., Storey, N., Wong, I., Siva, W., Gregor, N., Wright, D., and McDonald, G., 2004, Earthquake-hazards scenario for a M7 earthquake on the Salt Lake City segment of the Wasatch fault zone, Utah: Utah Geological Survey Special Study 111 DM, 59 p., 6 plates (compact disk).

Singh, S.K, Mena, E., and Castro, R., 1988, Some aspects of source characteristics of the 19 September, 1985 Michoacan earthquake and ground motion amplification in and near Mexico City from strong ground motion data: Bulletin of the Seismological Society of America, v. 78, p. 451-477.

Spudich, P., Joyner, W. B., Lindh, A. G., Boore, D. M., Margaris, B. M., and Fletcher, J. B., 1999, SEA99: A revised ground motion prediction relation for use in extensional tectonic regimes: Bulletin of the Seismological Society of America, v. 89, p. 1156-1170.

U.S. Geological Survey Staff, 1990, The Loma Prieta, California, earthquake: An anticipated event: Science, v. 247, p. 286-293.

U.S. Geological Survey, 1999, An assessment of seismic monitoring in the United States: Requirements for an Advanced National Seismic System: U. S. Geological Survey Circular 1188, 55 p.

Wong, I., Silva, W., Olig, S., Thomas, P., Wright, D., Ashland, F., Gregor, N., Pechmann, J., Dober, M., Christenson, G., and Gerth, R., 2002a, Earthquake scenario and probabilistic ground shaking maps for the Salt Lake City, Utah, metropolitan area: Utah Geological Survey Miscellaneous Publication MP-02-5, 50 p., 9 plates.

Wong, I., Silva, W., Gregor, N., Wright, D., Ashland, F., McDonald, G., Olig, S.,

Christenson, G., and Solomon, B., 2002b, Earthquake scenario ground shaking maps for the central Wasatch Front, Utah: Proceedings of the 7th U.S. National Conference on Earthquake Engineering, Boston, Mass., July 21-25, 2002, (compact disk).